ELSEVIER

Chemical Physics 222 (1997) 299–313

Chemical Physics

Vibrational study by inelastic neutron scattering, infrared absorption and Raman scattering of potassium, rubidium and cesium dihydrogenarsenate crystals: Comparison with thallium dihydrogenarsenate

Nicole Le Calvé *, Bernadette Pasquier, Zahra Ouafik

Laboratoire de Spectrochimie Infrarouge et Raman, Centre National de la Recherche Scientifique, 2 rue Henri Dunant, F-94320 Thiais, France

Received 12 May 1997

Abstract

The vibrational study of polycrystalline potassium, rubidium and cesium dihydrogenarsenates, KH_2AsO_4, RbH_2AsO_4 and CsH_2AsO_4, has been undertaken in the 20–4000 cm^{-1} range. The inelastic neutron scattering spectra obtained at 20 K allow a precise assignment of the OH vibrations. The infrared absorption and Raman scattering spectra of the paraelectric and ferroelectric phases have been analyzed. The three compounds are isomorphous with KH_2PO_4. The results are compared to those obtained for the thallium dihydrogenarsenate TlH_2AsO_4. In all compounds the proton dynamics appear weakly coupled to heavy atoms motions. The order–disorder transition at T_c is associated to relaxational motions of anions and protons in the tetragonal potassium, rubidium and cesium dihydrogenarsenates and to collective reorientational motions of anions in monoclinic thallium derivative. The spectroscopic features show the participation of cations K^+, Rb^+ and Cs^+ to the dynamics of the three-dimensional lattice in both phases. In contrast, heavy-cation Tl^+ motions are decoupled from the dynamics of hydrogen bond layers. No correlation between ordering of lattice and OH stretching wavenumber is observed. © 1997 Elsevier Science B.V.

1. Introduction

Potassium, rubidium and cesium dihydrogenarsenates KH_2AsO_4 (KDA), RbH_2AsO_4 (RDA) and CsH_2AsO_4 (CDA) undergo a paraelectric–ferroelectric phase transition at T_c. After partial structural studies [1,2] it was assumed that these compounds are isomorphous with KH_2PO_4 (KDP). In the paraelectric and ferroelectric phases, the hydrogen bonds built up a three-dimensional network [3]. Above T_c, the oxygen atoms of the hydrogen bonds are related by an axis C_2, which implies that the protons are disordered between two symmetrical positions. The protons are ordered below T_c. The paraelectric phase is characterized by the occurrence of a Raman low-frequency mode, a 'pseudo soft-mode ', the collective or relaxational origin of which being still widely discussed [4–12]. Such spectroscopic feature is also observed in the case of the antiferroelectric derivative $NH_4H_2AsO_4$ [13].

Thallium dihydrogenarsenate TlH_2AsO_4 (TDA) crystallizes in a monoclinic two-dimensional network ($P2_1/a$) [14], the hydrogen bonds setting up

* Corresponding author.

PII S0301-0104(97)00210-3

parallel layers as in the thallium (TlH_2PO_4, TDP) [15] and cesium (CsH_2PO_4, CDP) [16] phosphates. In the paraelectric phase, above T_c, half of the hydrogen bonds are disordered with the proton statistically located at the centre of the O · · · O distance [14]. Below T_c, the ordering of all hydrogen bonds leads to a doubling of the unit cell [17–19]. Moreover, the 'pseudo soft-mode' is not observed in the spectra of TDA. These facts suggest some questions concerning the dynamics of the proton in the two different crystalline organisations, the collective or relaxational nature of the 'pseudo soft-mode' and the respective participation of proton, cation and anion in the ordering of lattice at T_c.

Thus, a complete assignment of the OH vibrations is required to know the potential function governing the proton dynamics. The importance of coupling between the protons along the chains and between light and heavy atoms have to be investigated and compared inside the two different crystalline networks.

Inelastic neutron scattering (INS) provides specific information concerning the proton dynamics. The scattering cross-section of the hydrogen atom is more than one order of magnitude greater than those of the other atoms (As, O) and the INS intensity is directly proportional to the mean square amplitude of the proton displacement. Infrared and Raman spectroscopies allow us to set up the behaviour of cations and anions, emphasizing the relationship with the two- or three-dimensionality of the hydrogen-bonded systems.

Many infrared and Raman studies of KDA, RDA, CDA and their deuterated homologues have been published [12,20–28]. Few of them concern the vibrations of the OH group [20,21,27]. So far, as far as we know, no inelastic neutron scattering data on these arsenate salts has been published to date.

We investigated the infrared and Raman spectra of polycrystalline KDA, RDA and CDA in the 10–4000 cm^{-1} range in the paraelectric phase at 300 K and in the ferroelectric phase at 20 and 100 K. The INS spectra were recorded at about 20 K. The spectroscopic results are discussed with regard to those recently obtained for TDA [29].

2. Experimental

The compounds KDA, RDA and CDA were prepared from aqueous solution of potassium, rubidium and cesium carbonate, respectively, with a slight excess of arsenic acid H_3AsO_4. The compounds were precipitated by ethanol and dried under vacuum. A weak absorption near 3000 cm^{-1} could indicate the presence of H_2O or the formation of a very small amount of hydrates.

The infrared absorption spectra of mulled crystalline powder in paraffin oil were recorded on a Perkin-Elmer 983 spectrometer in the 200–4000 cm^{-1} range with a spectral resolution of 3–6 cm^{-1}. In the 20–400 cm^{-1} range, a Bruker FTIR 113V spectrometer was used with a spectral resolution of 2 cm^{-1}.

Raman spectra were obtained using a triple monochromator RTI 30 Dilor apparatus equipped with an Argon ionised Spectra-Physics (laser excitatrice line 514.5 nm). The Raman signal can be detected down to 5 cm^{-1}. The spectral resolution was better than 2 cm^{-1}, and about 4 cm^{-1} below and above 1300 cm^{-1}, respectively. The samples were sealed in glass tubes under helium atmosphere.

Conventional helium liquid cryostats were used for cooling samples down to 20 K.The temperature of the holder was stabilized within ± 2 K.

The INS spectra of polycrystalline samples of KDA (5.32 g), RDA (10.21 g), CDA (11.77 g) and TDA (8.03 g) were carried out on the TFXA spectrometer at the ISIS pulsed neutron source facility (Rutherford Appleton Laboratory, U.K.). The spectra of TDA give a better insight of the low wavenumber range relative to that published in [29]. The temperature was about 20 K. The energy resolution $\Delta E/E$ was $\sim 2\%$.

Fig. 1. Infrared (IR), Raman (R) and inelastic neutron scattering (INS) spectra of polycrystalline KH_2AsO_4 (KDA), RbH_2AsO_4 (RDA) and CsH_2AsO_4 (CDA) at 300 and 20 K between 10 and 500 cm^{-1}. (The INS intensities are not normalized between them.) +: laser plasma lines.

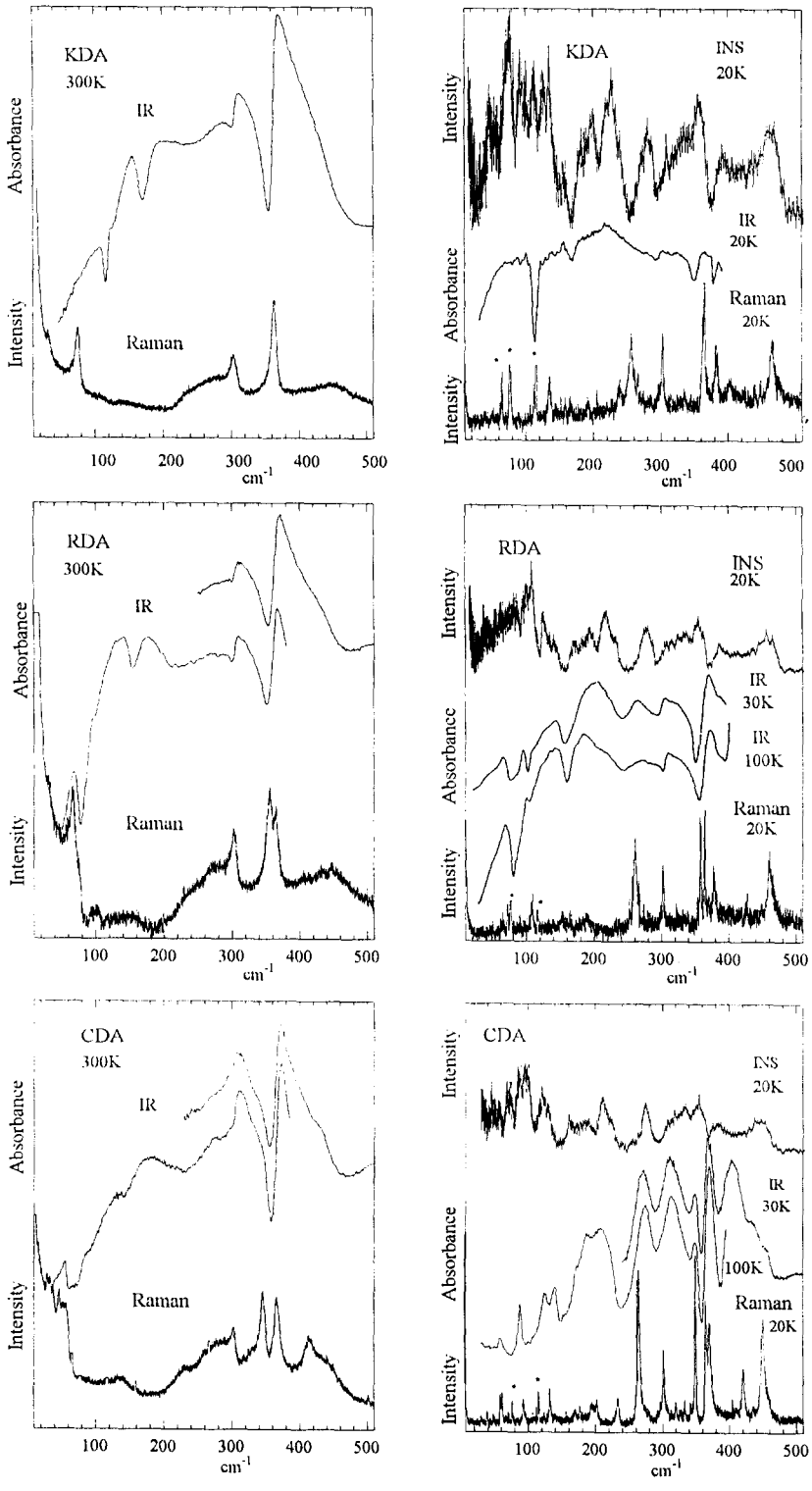
KDA
300K
IR
Raman
Absorbance
Intensity
100
200
300
400
500
cm-1
KDA
INS
20K
IR
20K
Raman
20K
RDA
300K
IR
Raman
RDA
INS
20K
IR
30K
IR
100K
Raman
20K
CDA
300K
IR
Raman
CDA
INS
20K
IR
30K
100K
Raman
20K

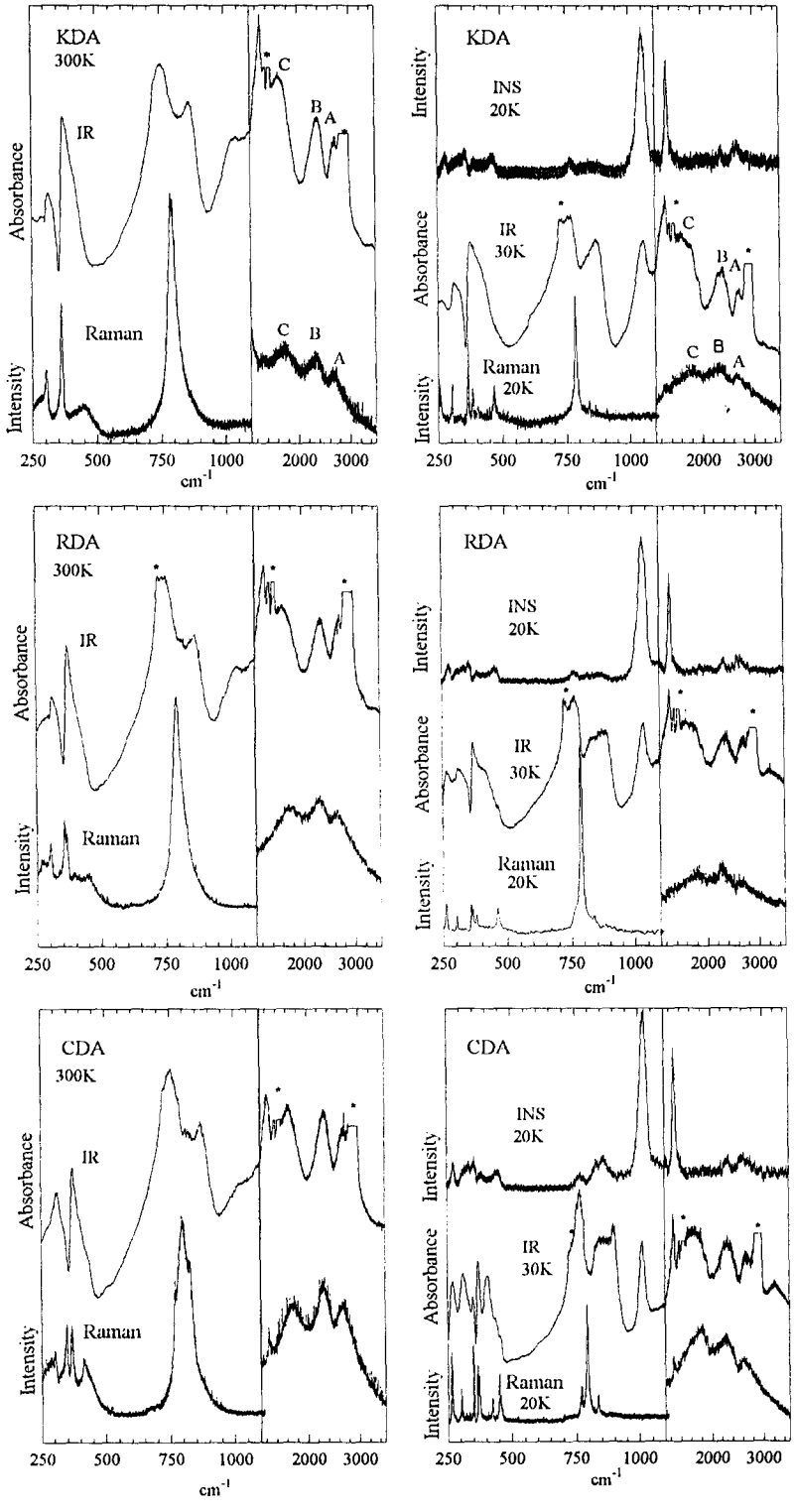
KDA
300K
IR
Raman
Absorbance
Intensity
C
B
A
250 500 750 1000 2000 3000
cm-1
KDA
INS
20K
IR
30K
Raman
20K
RDA
300K
RDA
CDA
300K
CDA

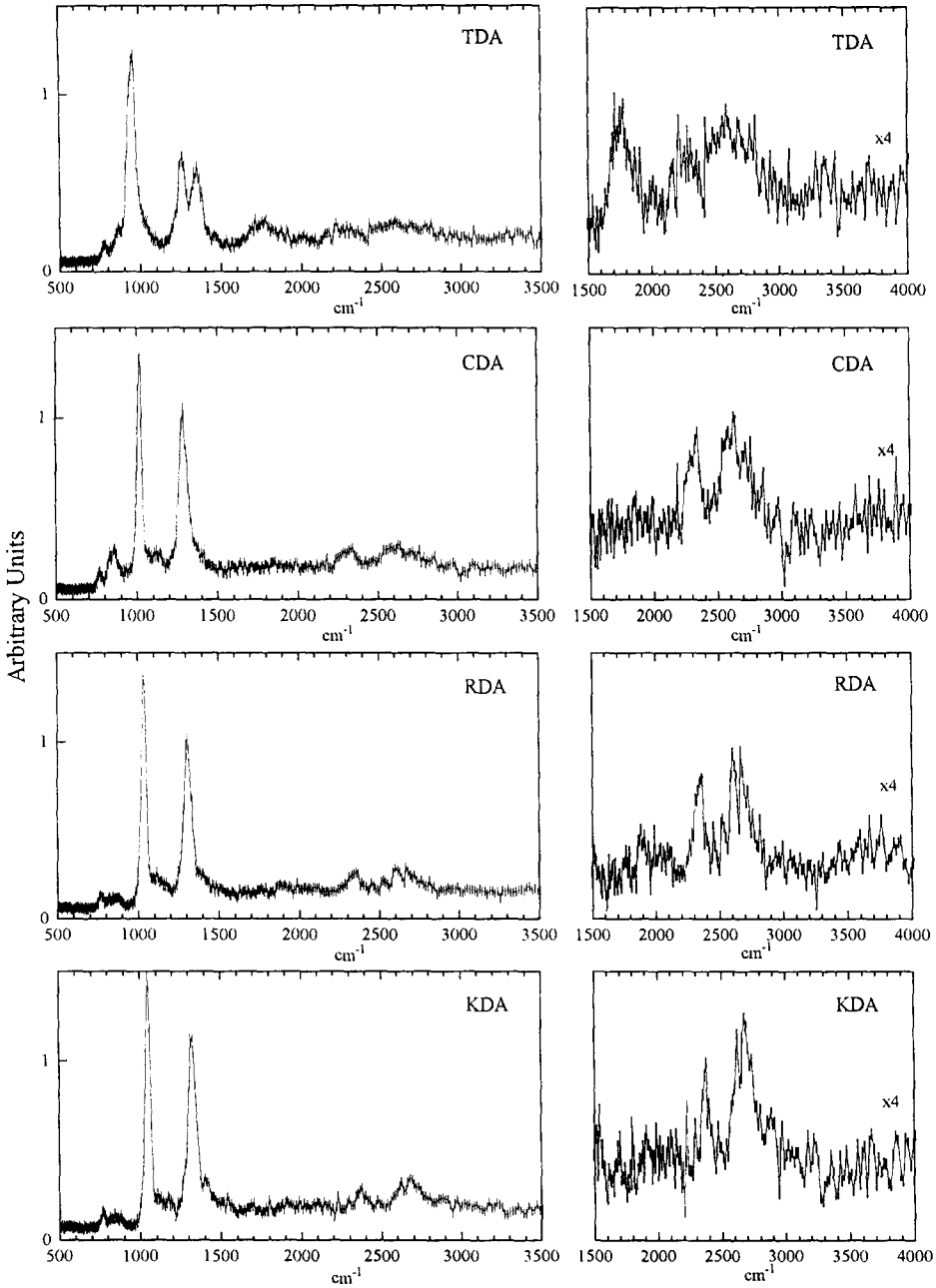

Fig. 3. Comparison of inelastic neutron scattering (INS) spectra of polycrystalline KH_2AsO_4 (KDA), RbH_2AsO_4 (RDA), CsH_2AsO_4 (CDA) and TlH_2AsO_4 (TDA) at 20 K in the 500–4000 cm^{-1} range. (The INS intensities are normalized relative to 1 mol H).

Fig. 2. Infrared (IR), Raman (R) and inelastic neutron scattering (INS) spectra of polycrystalline KH_2AsO_4 (KDA), RbH_2AsO_4 (RDA) and CsH_2AsO_4 (CDA) at 300 and 20 K between 250 and 4000 cm^{-1}. +: absorption of paraffin oil.

Table 1
Infrared (IR), Raman (R) and inelastic neutron scattering (INS) wavenumbers (cm^{-1}) and assignment to the external vibrations of paraelectric and ferroelectric phases of KH_2AsO_4 (KDA), RbH_2AsO_4 (RDA) and CsH_2AsO_4 (CDA)

KDA [a]					RDA [a]					CDA [a]					Assignment [b]	Series	
IR 300 K	R 300 K	IR 30 K	R 20 K	INS 20 K	IR 300 K	R 300 K	IR 30 K	R 20 K	INS 20 K	IR 300 K	R 300 K	IR 30 K	R 20 K	INS 20 K			
	33 w	25 w	25 vw			30 w	30?	32 vw			30 vw		30 vw		R_T	VI	
			50 w	46					40		37 w		39 w	42	T_T, T_M	V	
	67 sh		60 w	56		57 sh			55		47 w		49 w	45			
74 sh	75		78 m	77		67 m	65 sh	62 w			56 m, b		59 w	57	T_M, T_T, R_T	III	
			90 w	93			90 sh	90 w, b	95					90			
116 [c]		121 [c]			78 [c]					65 [c]					T_M	II′	
	110 w, b		113 m	112		76 sh	72 m	73 m	72		65 sh	60 m	62 m	70	T_M	II	$\delta_{O\cdots O}$
128 w			126 vw	127			130 sh				120 w, b	126 m	124 vw	122			
	140 w, b		136 m	135	97 sh	100 w, b	102 m	109 m	109	100 w	90 w, b	88 m	94 w	100	T_M, T_T	IV	
	160 w, b	163 m	165 w	158		150 w, b	147 m	154 w	160		135 w,b	142 m	132 w	130	T_M, T_T, R_T	I	
170 [c]					155 [c]					135 [c]					T_M, T_T, R_T	I′	
				178													
			192 w, b	200				188 w, b	195			180 sh	170 w,b	165			
190 s,b		200 s,b		219	160 s, b		206 s, b	216 w, b	217	176 s, b		186 s	195 w	185			$\nu_{O\cdots O}$
												207 s	202 w	211			
	238 w, b	223 s, b	226 sh	227	230 sh	230 w, b	230 sh	236 w, b	230		230 w, b		223 w	223			

[a] s = strong; m = medium; w = weak; sh = shoulder; b = broad.
[b] Rotational (R_T) and translational (T_T) motions of tetrahedra, and translational motions (T_M) of cation.
[c] Peak of transmission due to a Fano effect.

Table 2
Infrared (IR), Raman (R) and inelastic neutron scattering (INS) wavenumbers (cm^{-1}) and assignment to the internal modes of the AsO_4 group in the paraelectric and ferroelectric phases of KH_2AsO_4 (KDA), RbH_2AsO_4 (RDA) and CsH_2AsO_4 (CDA)

KDA [a]					RDA [a]					CDA [a]					Assignment [b]
IR 300 K	R 300 K	IR 30 K	R 20 K	INS 20 K	IR 300 K	R 300 K	IR 30 K	R 20 K	INS 20 K	IR 300 K	R 300 K	IR 30 K	R 20 K	INS 20 K	
280 b	270 b		255 m		290 b	280 b	300 b	261 m	277	267 sh	280 b	274 m	264 s	275	
		208 sh		280											
300 [b]	303 m		302 m		300 [b]	303 m	300 [b]	303 m		300 sh	300 m	300 sh	301 m		
		310 mb		309			310 m		306			312 m	320 w	315	ν_2
		311 m, b	334 w	335				335 w	336				334 w	335	
			363 m			356 m		358 s			346 m		350 s		and
354 [b]	363 s	357 [b]		358	355 [b]		356 [b]		354	355 [b]		349 m		354	
			366 s			365 m		365 s			367 m		365 m		
370 s, b		370 s, b	383 m	393	360 s, b		370 m, b	379 m	386	360 s, b	360 m, b	370 s	370 m	380	ν_4
	400 w		404 w	419		410 w, b	410 m, b		410		418 m	405 m	421 m		
440 sh	452 w, b		440 w	435	440 sh	445 w, b	466 w	462 m	460	431 sh	455 w, sh	440 sh	450 m	445	
			466 m	460				470 sh				460 sh	460 sh		
			504 vw		510 vw		540 vw					540 w			$\nu_2 + \nu_4$
							610 sh					615 sh			
												756 sh	760 m		
751 vs		760 vs		767	750 vs	772 sh	766 vs	765 w	762	750 vs	767 sh			770	ν_3
												764 vs	770 m		
							770 sh			780 sh		774 sh	780 sh		
	790 vs		784 vs			792 vs		787 vs	817		797 vs		793 vs		ν_1
		830 sh	837 w	837	820 sh	830 sh	840 sh	838 w	837	820 m	825 m	840 m	833 m	833	
860 s	860 sh	865 s		875			860 m					860 m	853 w	859	
					870 m	877 sh	880 s		870	870 s	880 sh	900 s	890 w		ν_3
											920 sh	920 vw	916 vw	930	

[a] See footnote [a] of Table 1.
[b] Peak of transmission due to a Fano effect.

Table 3
Infrared (IR), Raman (R) and inelastic neutron scattering (INS) wavenumbers (cm^{-1}) and assignment to the OH vibrations of paraelectric and ferroelectric phases of KH_2AsO_4 (KDA), RbH_2AsO_4 (RDA) and CsH_2AsO_4 (CDA) and comparison with the low-temperature phase of TlH_2AsO_4 (TDA)

KDA [a]					RDA [a]					CDA [a]					TDA	Assignment
IR	R	IR	R	INS	IR	R	IR	R	INS	IR	R	IR	R	INS	INS	
300 K	300 K	30 K	20 K	20 K	300 K	300 K	30 K	20 K	20 K	300 K	300 K	30 K	20 K	20 K	20 K	
1015 m		1050 s	(1036)	1050	1024 m		1034 s	(1026)	1035	1020 sh		1012 s	(1015)	1019	920	
															930	γ_{OH}
															952	
															976	
1165 sh		1160 sh		1180	1160 sh		1170 w		1120	1160 sh		1150 sh		1140		$\nu_3 + \nu_4$
		1240 sh	1245 w				1230 sh					1230 sh				
			(1298)					(1286)					(1265)		1245	
1283 s	1290 w	1300 s	1304 w	1320	1266 s		1284 s	1320 w	1303	1236 s	1250 w	1264 s	1260 w	1290		δ_{OH}
			(1239)									1288 sh	1290 vw		1345	
			(1329)					(1316)					(1292)			
560		*740*			*560*		*700*			*400*		*520*				
1670 s, b		1610 s, b			1650 s, b		1590 s, b			1630 s,b		1650 s,b	1580 sh		1760	'C'
1730 sh	1750 w	1780 s, b	1780 w			1760 w	1710 s, b	1780 w			1700 w		1750 w			
							1790 sh			1770 sh		1794 w	1795 w			
		1930 sh		1940			1910 sh		1920			1907 w		1880		$2\gamma_{OH}$
	2230 w		2330 w			2330 w		2280 w			2320 w		2280 w			
2380 s, b		2370 s, b		2280	2350 s,b		2360 s, b		2360	2330 s,b		2310 s,b		2330	2200	'B'
2560 [b]	2520 [b]	2590 [b]	2560 [b]		2560 [b]		2580 [b]			2530 [b]		2540 [b]	2510 [b]			$2\delta_{OH}$
2700 m,b	2690 w	2700 s	2690 w	2690	2680 s, b	2650 w	2680 s, b	2650 w	2670	2640 s, b	2680 w	2650 s,b	2630 w	2640	2600	'A'

( ): polarized Raman bands from Ref. [27]; *italic*: FWHH (cm^{-1}) of 'C' component.
[a] See footnote [a] of Table 1.
[b] Peak of transmission due to a Fano effect.

3. Structural data

The temperature T_c is lower in the arsenates salts KDA, RDA and CDA, i.e. 95, 109 and 147 K, respectively [30] than in the corresponding phosphates KDP [30], RDP [30] and CDP [31], i.e. 123, 147 and 153 K, respectively. In contrast, in the thallium derivatives, T_c is higher in TDA (251 K) [32] than in TDP (229 K) [33], assuming an original behaviour of these two compounds relative to that of the other three arsenates.

Above T_c, the paraelectric phases of KDA, RDA and CDA belong to the tetragonal symmetry $I\bar{4}2d$ (D_{2d}) [1,34,35] with two entities in the primitive cell. Each tetrahedron (site symmetry S_4) is linked by short equivalent disordered hydrogen bonds located on a site C_2. Neutron diffraction data evidence two equivalent positions of H(D) atoms between tetrahedra [2,36]. The O · · · O distance, slightly longer in KDA (0.252 nm) [34] than in KDP (0.2495 nm) [37], has not been determined in RDA and CDA.

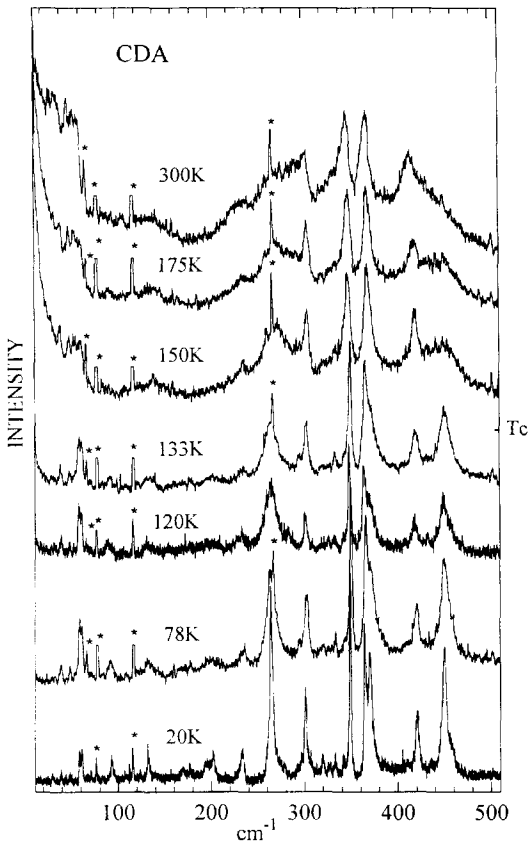

Fig. 4. Evolution of the Raman spectra of polycrystalline CsH_2AsO_4 (CDA) with temperature in the external and AsO_4 bending vibrations range. +: laser plasma lines.

The unknown ferroelectric phases of RDA and CDA are assumed to be isomorphous with the orthorhombic Fdd2 (C_{2v}) phase of KDP and KDA [1,2] with two formulas per unit cell. It should be underlined that CDA and CDP are not isostructural. Actually, the paraelectric and ferroelectric phases of CDP belong to the monoclinic system, $P2_1/m$ (C_{2h}) and $P2_1$ (C_2), respectively [16]. Unlike CDA, two kinds of hydrogen bonds exist in CDP, leading to a pseudo-unidimensional network [38] quasi-isostructural with TDP [39].

In the paraelectric phase at room temperature, TDA crystallizes in the monoclinic structure $P2_1/a$ (C_{2h}) with four formulas per unit cell [14], the O · · · O distances deduced from the spectroscopic results being likely shorter than 0.255 nm [29]. It is isomorphous with TDP [15,39]. Below T_c, by analogy with TDP, a centrosymmetrical structure would occur according to the antipolar character [40]. However, in the case of TDP, spontaneous polarisation [41] and SHG measurements [35] show an acentric structure. Elsewhere, the spectroscopic results on TDP and TDA suggested also a non-centrosymmetrical phase at about 100 K below T_c [29,42].

4. Vibrational analysis

The infrared and Raman spectra of the paraelectric and ferroelectric phases of KDA, RDA and CDA and the INS spectra of the ferroelectric phases are reproduced in Figs. 1 and 2 in the 10–500 and 250–3500 cm^{-1} range, respectively. The INS spectra of KDA, RDA, CDA and TDA in the 500–4000 cm^{-1} range are compared in Fig. 3. The Raman spectra in the 10–500 cm^{-1} range of CDA at different temperatures are illustrated in Fig. 4.

The assignments of the bands observed in the 10–250, 250–1000 and 1000–4000 cm^{-1} ranges, given in Tables 1–3, respectively, are roughly according to the previous studies [12,20–28]. Concerning the wavenumbers, the infrared and Raman spectra of KDA, RDA and CDA do not change steadily

from the paraelectric to the ferroelectric phase. Owing to the INS data at low temperature, a complete vibrational analysis of the arsenate salts may be achieved in the ferroelectric phase.

The factor group analysis in the tetragonal and orthorhombic phases leads to 23 and 30 internal and 10 and 15 external modes, respectively. Among the internal modes, 14 or 18 are provided by the AsO_4 group and 9 or 12 by the OH group. Generally, in this type of disordered hydrogen-bonded crystals, the AsO_4 modes do not obey to the selection rule of the crystalline symmetry [29], above T_c, according to a single well potential function of H atoms, on the vibrational times.

The external modes are due to translational and rotational motions of H_2AsO_4 anions and to the translational motions of cations.

4.1. External modes

In this type of hydrogen-bonded compounds, the external modes are usually observed below 300 cm^{-1} [18,29,42]. The translational and rotational motions of anions could be described as hydrogen bond stretching $\nu_{O\cdots O}$ and bending $\delta_{O\cdots O}$ modes. In the tetragonal phase, 9 Raman active and 6 infrared active vibrations are expected against 15 Raman active and 12 infrared active vibrations in the orthorhombic phase.

Above T_c, the $\nu_{O\cdots O}$ stretchings are related to the INS and broad infrared bands between 170 and 250 cm^{-1} (Fig. 1). The decrease of the $\nu_{O\cdots O}$ wavenumber going from KDA to CDA shows a lengthening of the hydrogen bond as the mass of cation increases (Table 1). That result will be confirmed by the study of OH vibrations. At low temperature, as shown in Fig. 1, the narrowing of infrared bands mainly due to hydrogen bond stretchings is well marked in the case of largest cation Cs^+.

Regarding the lower frequency range, the infrared spectra in the tetragonal phase can be analyzed according to a Fano effect [43] like a quasi-continuum interacting with two narrow levels at 116 and 170 cm^{-1} in KDA, 78 and 155 cm^{-1} in RDA, and 65 and 135 cm^{-1} in CDA (Fig. 1). The Raman spectra are characterized by important Rayleigh wings and narrow and broad bands near 75 and 150 cm^{-1}, respectively (Fig. 1). These bands have to be assigned to $O\cdots O$ bending modes. Below T_c, the ordering of lattice is manifested in the Raman spectra by the bandwidth narrowing and the vanishing of the wings of the Rayleigh line. As in the $\nu_{O\cdots O}$ range, the broad infrared characteristic features of paraelectric phase are maintained in KDA and RDA. The similar spectroscopic features observed in the three compounds allow us to make up six series of characteristic bands and to determine the assignments above and below T_c.

I and I': At 300 K, the Raman band of B_2 symmetry species [12,22,25,44] near 160, 150 and 135 cm^{-1} in the spectra of KDA, RDA and CDA (series I) (Fig. 1) were assigned to the B_2 optical mode, coupled with the protonic motion. The frequency ratios calculated from the reduced mass cation–anion are 0.89 for ν_{Cs^+}/ν_{Rb^+} and 0.76 for ν_{Rb^+}/ν_{K^+}. The experimental values are 0.90 and 0.94, respectively, showing a complex description of the mode with the nature of cation. In the same way, the 'negative' infrared bands observed at 170, 155 and 135 cm^{-1} in KDA, RDA and CDA (series I'), respectively, are related to relative motions of cations and anions.

II and II': The 'negative' bands at 116, 78 and 65 cm^{-1} (series II) are due to a purely translational motion of cation according to the experimental values of the ratios ν_{Cs^+}/ν_{Rb^+} and ν_{Rb^+}/ν_{K^+} (0.83 and 0.67, respectively) very close to the calculated ones (0.80 and 0.68, respectively) taking into account only the mass of cation and the very weak corresponding INS intensities. Such assignment is proposed for the broad Raman bands at same wavenumbers (series II').

III and IV: Due to experimental frequency ratios of 0.86 and 0.80 for ν_{Cs^+}/ν_{Rb^+} and ν_{Rb^+}/ν_{K^+}, the series IV is assigned to relative translational motions of cations and anions. In the series III, the experimental values of 0.83 and 0.89, respectively, can be explained by the participation of rotational motions of anions.

V: The INS signal detected near 40 cm^{-1} has to be associated to the low wavenumber mode expected in KDP and KDA [22] and observed in deuterated analogous RbD_2AsO_4 and KD_2AsO_4 at 33 and 45 cm^{-1}, respectively [25]. In the INS spectra of TDA, a narrow peak near 32 cm^{-1} was assigned to relative sliding of cations and anions [29].

VI: Finally, in the paraelectric phase, the weak Raman band near 30 cm^{-1} is assigned to rotational motion of tetrahedra.

Regarding the above analysis, some features could be emphasized. In KDA and RDA, the important bandwidth of infrared bands below T_c is associated to a residual dipolar disorder in the ferroelectric phase. However, in TDA, [29] and TDP [42], as in the tetragonal compounds, a residual disorder of lattice occurs down to about 100 K below T_c. Moreover, many external modes appear more sensitive to the nature of cation than to the ordering of crystal, revealing the participation of cations to the long-range interactions in the crystal. The motions of cations are implied in the dynamics of the whole H_2AsO_4 network, according to their INS activity. In contrast, in the thallium derivatives TDA and TDP, the translational motions of Tl^+ assigned to intense Raman bands near 40 cm^{-1} were unobserved in the INS spectra [29,42]. Likely due to the mass of cation, the Tl^+ modes are decoupled from the dynamics of the hydrogen bonds.

Finally, the spectrum of the ferroelectric phase of CDA is well structured below 100 K, the number of bands being consistent with the factor group analysis assuming isomorphism with KDP (Fig. 1; Table 1).

4.2. AsO_4 group vibrations

The stretching ν_1 and ν_3 and bending ν_2 and ν_4 modes are expected in the 1000–700 and 500–250 cm^{-1} ranges, respectively [24,25,29,45–47]. Their Raman and infrared activity in the factor groups D_{2d} and C_{2v} are given in Table 4. The weak INS intensity of the bands due to the vibrations of the AsO_4 group shows the decoupling of proton dynamics from those of heavy atoms.

Above T_c, concerning the stretching vibrations, the infrared and Raman spectra of KDA are characteristic of the crystallographic site symmetry S_4, the intense bands at 790 cm^{-1} in Raman and 751 and 860 cm^{-1} in infrared being assigned to ν_1 (1A) and ν_3 (1B + 1E) modes, respectively (Table 2). The lattice correlation effect increases from KDA to CDA.In this last compound, the five Raman bands expected in that wavenumber range are observed (Table 2). Below T_c, at 20 K, the expected number of bands ($2\nu_1 + 6\nu_3$) is well observed in the case of CDA (Table 2). Actually, the narrow band at 900 cm^{-1} in the infrared spectra of CDA, assigned to a ν_3 component is scarcely observed in the spectra of KDA and RDA as in the polarized Raman spectra [25]. Again, the infrared and Raman bands of KDA can be assigned to the AsO_4 vibrations only in terms of the site symmetry C_2.

Table 4
Group factor analysis of normal modes of AsO_4 group in the tetragonal and orthohombic phases

		Site group		Factor group ($Z = 2$)	
	T_d	S_4	C_2	D_{2d}	C_{2v}
ν_2	E(R)	A(R)	A(R,IR)	A_1(R)	A_1(R,IR)
				A_2	A_2(R)
		B(R,IR)	A(R,IR)	B_1(R)	A_2(R)
				B_2(R,IR)	A_1(R,IR)
ν_3, ν_4	F_2(IR,R)	B(R,IR)	A(R,IR)	B_1(R)	A_2(R)
				B_2(R,IR)	A_1(R,IR)
		E(R,IR)	2B(R,IR)	2E(R,IR)	$2B_1$(R,IR)
					$2B_2$(R,IR)
ν_1	A_1(R)	A(R)	A(R,IR)	A_1(R)	A_1(R,IR)
				A_2	A_2(R)

In the tetragonal phase, the infrared spectra of the bending modes of AsO_4 group, between 250 and 500 cm^{-1}, present typical features which could be analyzed as Fano effects between a broad component centered near 360 cm^{-1} and two narrow levels corresponding to the Raman bands near 300 and 350 cm^{-1} (Fig. 2). Assuming a coupling with the 'ferroelectric mode' via the B_2 anti-translational cation–anion motion, the ν_4 (B_2) mode was assigned to the band near 280 cm^{-1} [12]. However, after Raman polarization studies, that latter band belongs to a A_1 symmetry species due to a ν_2 component [21,22,25]. Then, the mode ν_4 (B_2) is rather related to the broad infrared feature around 370 cm^{-1}, the narrow Raman bands near 300 and 350 cm^{-1} and the broad components near 420 cm^{-1} being assigned to ν_2 and ν_4 modes, respectively [12,18,24,26]. Only in the case

of CDA, all expected components are observed but the detailed assignment is not achieved.

In the Raman spectra, a steady narrowing of the bands is observed in the ferroelectric phase (Fig. 2). In the infrared spectra of KDA and RDA, the Fano-type features evidenced at 300 K are yet observed at 30 K, near 300 and 360 cm^{-1} (Fig. 2) whereas the coupling between the ν_4 vibrations and the 'ferroelectric mode' of proton cannot be invoked. The occurrence of a residual local disorder in the ferroelectric phase, as suggested in the case of O · · · O vibrations and AsO_4 stretching modes, reveals also the sensitivity of the AsO_4 bending vibrations to the surrounding organisation. That effect is likely favored by interactions with the H-bond vibrations lying in the near wavenumber range. A similar behaviour of AsO_4 bending modes was observed in the infrared spectra of the totally disordered paraelastic phase of TDA [45], the disorder being essentially related to reorientational motions of anions [47].

Regarding the weak INS intensities of the AsO_4 modes, local intramolecular couplings related to covalent bonds vanish and are superseded by long-range interactions in the crystal. As observed in the case of external modes and AsO_4 stretching modes, these interactions increase with the mass of cation. That is manifested by the splitting of the two Raman components near 350 cm^{-1} that increases from 3 cm^{-1} in KDA to 7 cm^{-1} in RDA and 21 cm^{-1} in CDA.

4.3. OH group vibrations

The wavenumbers and the assignments of the OH vibrations are gathered in Table 3. These modes give rise to intense features in the INS spectra.

For each OH vibrator, three vibrations are defined corresponding to one stretching ν_{OH} and two bendings δ_{OH} and γ_{OH} ($\nu_{d(1)}$ and $\nu_{d(2)}$ after [27]). The frequency of these vibrations are very sensitive to the O · · · O distance [48]. In the paraelectric phase of KDA, the O · · · O distance is 0.252 nm [34]. Such a value allow the hydrogen bond strength to be evaluated as 'strong'. In the isomorphous arsenates, the O · · · O distances are expected to be similar. In an X-ray study of TDA, the O · · · O distances vary from 0.270 to 0.250 nm [39] but the spectroscopic results permit to reduce these distances to about 0.250–0.255 nm [29].

Raman studies in polarized light of the ferroelectric phase of KDA, RDA and CDA [27] have shown very close wavenumbers corresponding to the different symmetry species of the OH bending modes according to very weak interactions between the proton motions.

The INS spectra of KDA, RDA and CDA in the ferroelectric phase allow us to assign the δ_{OH} and γ_{OH} to strong bands at 1320, 1303 and 1290 cm^{-1} and 1050, 1035 and 1019 cm^{-1}, respectively (Figs. 2 and 3; Table 3). The corresponding infrared bands are rather strong.

The δ_{OH} and γ_{OH} wavenumbers decrease from KDA to CDA and increase below T_c. In the case of isomorphous structure, that result indicates a lengthening of the O · · · O distance with the mass of cation such as $R_{O \dots O}$ (CDA) > $R_{O \dots O}$ (RDA) > $R_{O \dots O}$ (KDA) and a strengthening of the H-bonds in the ordered phase. Moreover, in the case of CDA, the infrared bandwidths of the OH bending modes present a critical behaviour at T_c as shown in Fig. 5. The large increase of the bandwidths in the disor-

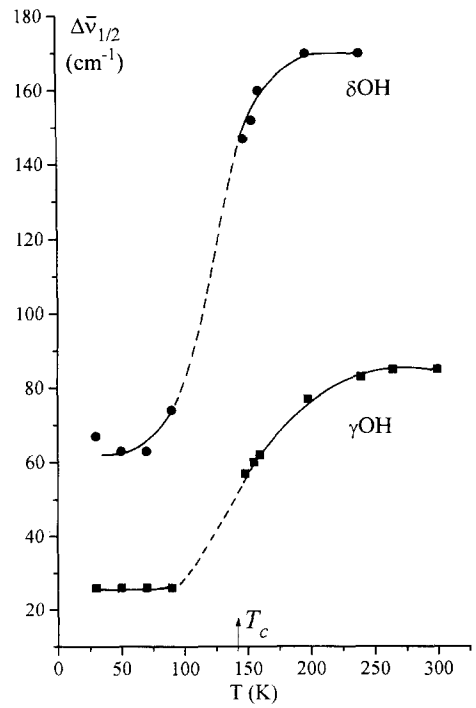

Fig. 5. Evolution of δ_{OH} and γ_{OH} infrared bandwidths (FWHH) vs. temperature in polycrystalline CsH_2AsO_4.

dered phase emphasizes a great sensitivity of the proton dynamics in the OH bending modes to the surrounding organisation of the crystal.

The INS and infrared bandwidths due to δ_{OH} modes are broader than the corresponding γ_{OH} bands even at low temperature. An electrical coupling between ν_{OH} and δ_{OH} modes, favored by the proximity of their frequencies, could be suggested. That interaction decreases from KDA to CDA as δ_{OH} wavenumber decreases, leading concurrently to the narrowing of bandwidth (Fig. 2).

In the INS spectra of the low-temperature phase of TDA, the δ_{OH} and γ_{OH} bands are split into two components: 1245–1345 and 930–952 cm^{-1}, respectively [29] (Fig. 3). These important splittings are assigned to the two kinds of H-bonds in TlH_2AsO_4 by analogy with CsH_2PO_4 [49]. Moreover, the ($\delta_{OH}-\gamma_{OH}$) splitting is larger in TDA ($\cong$ 340 cm^{-1}) than in the other three compounds ($\cong$ 270 cm^{-1}), characterizing the OH bending coordinates involved in three- or two-dimensional hydrogen bond structures. That behaviour is also observed in phosphate salts, the wavenumber splitting going from 256 cm^{-1} in KDP [50] to 340 cm^{-1} in TDP [42].

As anticipated from their O $\cdots$ O distances, the infrared and Raman spectra of arsenate salts present the classical 'ABC' profile for short hydrogen bonds in the 1400–3000 cm^{-1} range (Fig. 2) [48]. From polarized Raman spectra of dihydrogen phosphates and arsenates [27], the 'AB' splitting has been explained by a Fano-type resonance between a wide level ν_{OH} and a narrow one due to $2\delta_{OH}$. This interpretation is also convenient to explain the doublet ν_{OD} observed in the spectra of deuterated homologues of the KDP family [27]. Below T_c, the infrared 'C' component of KDA, RDA and CDA presents an important broadening relative to the paraelectric phase, the other two components being unchanged. Actually, the 'C' bandwidth increases by about 30% as the temperature decreases from 300 to 20 K. In opposite, in TDA, the corresponding bandwidth slightly decreases only from 280 cm^{-1} at 300 K to 260 cm^{-1} at 20 K.

In the ν_{OH} frequency range, due to the Debye–Waller factor, the INS spectra of hydrogen-bonded compounds are generally weak and poorly-resolved and muddled by overtones and combinations of OH bendings (Fig. 3). However, in the INS spectra of TDA the 'C' component is well defined at 1760 cm^{-1}. A similar profile appears in the INS spectra of TlH_2PO_4 [42] and $PbHPO_4$ [51]. These INS features suggest that the 'C' component would be rather related to the ν_{OH} mode. That assignment would reveal a weakening of the OH bond, due to an increase of the ionic character of the $O^{-\delta} \cdots H^{+\delta} \cdots O^{-\delta}$ bond as proposed in carbonate salts [52]. It would result in a disorder of proton at low temperature, manifested by the broad infrared features of the 'C' component in the polar phase. However, no tunneling effect is detected in the INS spectra above 30 cm^{-1}. In TDA, the spectroscopic behaviour of the 'C' component could indicate a different potential function governing the proton dynamics, ensuring a more covalent character of the OH bond. An alternative would be the occurrence of a ν_{OH} component becoming infrared active below T_c. Actually, polarization studies shown that the frequency splittings due to correlation effect are greater for the 'C' component than for the 'A' and 'B' [27].

4.4. Central mode

The behaviour of the low-frequency Raman spectra of CDA with temperature is illustrated in Fig. 4. Unlike the external modes, the Rayleigh wings present a critical behaviour as the temperature falls. A relaxational mechanism was assumed in ferroelectric and antiferroelectric crystals of the KDP family to explain the anomalous large dielectric constant below T_c [53,54], the reflectivity spectra [13,55] and the Raman quasi-elastic component [6,10,56]. The central mode should imply relaxational motions of anions and protons inside the H-bond network. These motions could be associated to multidomain walls displacements in the disordered phase. As shown for KDA [54,56] and CDA [57], the relaxation times of dipoles increases as the temperature decreases. Simultaneously, the broadening of the Rayleigh line disappears. The phase transition is achieved when the mobility of domain walls strongly decreases.

No characteristic Rayleigh line broadening is detected in the spectra of the paraelectric phase of TDA [29]. Due to the doubling of the cell at T_c, no soft mode associated with an optical phonon at the Brillouin zone boundary is expected which confirms the relaxational character of the transition in the

antiferroelectric crystal $NH_4H_2PO_4$. This fact, associated with the decoupling of Tl^+ translations from the vibrations of the hydrogen bonds, shows the original dynamics of the lattice in the thallium arsenate and phosphate derivatives. There is no evidence that collective proton transfer occurs in these compounds. In the thallium salts, the mechanism of the order–disorder transition was mainly associated to collective reorientational motions of AsO_4. It is suggested that the dynamics of protons and tetrahedra are concerted in the ordering of the lattice. However, in the quasi-isomorphous crystal CsH_2PO_4, a relaxational motion of proton has been invoked to explain the INS intensity observed at low frequency in the polarized spectra of the ferroelectric phase [49].

5. Conclusions

The vibrational behaviour of the three arsenates KDA, RDA and CDA confirms the isomorphism of the paraelectric and ferroelectric phases and shows the lengthening of the O · · · O distances from KDA to CDA. The results were compared to those obtained for the monoclinic crystal TDA in relation with the three- or two-dimensional crystalline organisation of the H-bonds and the nature of cation.

In all cases, the weak INS intensities of the AsO_4 internal modes show a decoupling of the proton dynamics from those of surrounding atoms. The intermolecular couplings result from dipolar long-distance interactions and appear favored in the case of the large cation Cs^+.

Due to INS results, a complete assignment of the OH vibrations is given. Whatever the crystalline structure, no significant change is observed at T_c concerning the wavenumber of the ν_{OH} stretching. No tunneling effect is detected at least above 30 cm^{-1}. No correlation between the ordering of lattice and ν_{OH} wavenumber is evidenced in contrast to the great sensitivity of the δ_{OH} bandwidth to the surrounding disorder in the tetragonal compounds. The spectroscopic behaviour of OH stretching mode depends on the crystalline organisation revealing different rate of ionic character of the OH bond. A detailed knowledge of the proton dynamics is required for establishing the relationship between the crystalline structure of a system and the proton transfer rate.

The translational motions of K^+, Rb^+ and Cs^+ are implied in the dynamics of the lattice. In contrast, the Tl^+ translations are decoupled from the H_2AsO_4 motions. The participation of cations to the dynamics of the hydrogen bonds depends on the nature of cation and can be related to the crystalline organisation. Thus, in KDP family compounds, the three-dimensional H-bond network occurs if the volume (or the mass) of anion is large relative to that of cation (KDP, RDP, KDA, RDA, CDA). The two-dimensional structure exists in heavy-cation salts such as CDP, TDP and TDA.

Finally, the ordering of the lattice at T_c should be monitored by dipolar relaxational motions of ions and protons in the three-dimensional H-bond network or by collective reorientational motions of anions inside the hydrogen bond layers.

Acknowledgements

We wish to thank Mrs. R. Baddour-Hadjean and N. Leygues of the LASIR-CNRS, Thiais, for their help in the neutron scattering experiments.

References

[1] Landolt–Börnstein, vol. 3, Ferroelectric and Antiferroelectric Substances, Springer, Berlin, 1969, p.139.
[2] W.J. Hay, R.J. Nelmes, Ferroelectrics 14 (1976) 599.
[3] J.C. Slater, J. Chem. Phys. 9 (1941) 16.
[4] K. Kobayashi, J. Phys. Soc. Jpn. 24 (1968) 497.
[5] N. Lagakos, H.Z. Cummins, Phys. Rev. B 10 (1974) 1063.
[6] M. Tokunaga, Y. Tominaga, I. Tatsuzaki, Ferroelectrics 63 (1985) 171.
[7] Y. Takagi, Ferroelectrics 46 (1983) 245.
[8] T. Yagi, M. Arima, A. Sakai, J. Phys. Soc. Jpn. 59 (1990) 1430.
[9] M. Tokunaga, T. Matsubara, Ferroelectrics 72 (1987) 175.
[10] M. Tokunaga, I. Tatsuzaki, Phase Transitions 4 (1984) 97.
[11] R. Blinc, B. Zeks, Ferroelectrics 7 (1987) 193.
[12] P. Simon, F. Gervais, E. Courtens, Phys. Rev. B 37 (1988) 1969.
[13] B. Wyncke, F. Brehat, H. Arbouz, Phys. Status Solidi B 134 (1986) 523.
[14] T.V. Narasaiah, R.N.P. Choudhary, N.C. Shivaprakash, Proc. Indian Acad. Sci. (Chem. Sci.) 100 (1988) 447.
[15] R.J. Nelmes, R.N.P. Choudhary, Solid State Commun. 38 (1981) 321.
[16] B. Marchon, A. Novak, J. Chem. Phys. 78 (1983) 2105 and references therein.

[17] R.J. Nelmes, Solid State Commun. 39 (1981) 741.
[18] K.S. Lee, D.H. Ha, Phys. Rev. B 48 (1993) 73.
[19] F. Milia, Ferroelectrics 20 (1978) 229.
[20] E. Wiener, S. Levin, I. Pelah, J. Chem. Phys. 52 (1978) 2881.
[21] H. Ratajczak, J. Baran, V. Videnova, Z. Mielke, M. Jarosz, 20th Int. Colloq. Spectrosc., Prague, 1977.
[22] D.K. Agrawal, C.H. Perry, Proc. 2nd Int. Conf. on Light Scattering in Solids, M. Balkanski (Ed.), Flammarion, Paris, 1971, p.429.
[23] H. Hammer, Proc. 2nd Int. Conf. on Light Scattering in Solids, M. Balkanski (Ed.), Flammarion, Paris, 1971, p.425.
[24] R.S. Katiyar, J.F. Ryan, J.F. Scott, Phys. Rev. B 4 (1971) 2635.
[25] R.P. Lowndes, N.E. Tornberg, R.C. Leung, Phys. Rev. B 10 (1974) 911.
[26] I. Laulicht, R. Ofek, J. Raman Spectrosc. 4 (1975) 41.
[27] E.V. Chisler, V.Yu. Davydov, J. Mol. Struct. 177 (1988) 231.
[28] R.C. Leung, N.E. Tornberg, R.P. Lowndes, J. Phys. C: Solid State Phys. 9 (1976) 4477.
[29] Z. Ouafik, N. Le Calvé, B. Pasquier, Chem. Phys. 194 (1995) 145.
[30] E. Dubler, Z. Kopajtic, Thermal. Anal., Proc. 6th Int. Conf. Thermal Anal., Hemmingen W. Birkhäuser, Vol. 2, 1980, p. 371.
[31] A. Levstik, R. Blinc, P. Kadaba, S. Cizikov, C. Filipic, Solid State Commun. 16 (1975) 1339.
[32] K. Irokawa, M. Komukae, T. Osaka, Y. Makita, J. Phys. Soc. Jpn. 63 (1994) 1162.
[33] T. Matsuo, H. Suga, Solid State Commun. 21 (1977) 923.
[34] J. Shankar, V.M. Padmanabhan, Crystallography and Crystal Perfection, Academic Press, New York, 1964, p.273.
[35] G.M. Loiacono, J. Ladell, W.N. Osborne, J. Nicolosi, Ferroelectrics 14 (1976) 761.
[36] M. Matsuda, N. Niimura, S. Kawano, A. Nonaka, N. Yamada, J. Phys. Soc. Jpn. 57 (1988) 3824.
[37] N.S.J. Kennedy, R.J. Nelmes, J. Phys. 13 (1980) 4841.
[38] V. Videnova, A. Drabinska, J. Baran, J. Mol. Struct. 156 (1987) 1.
[39] S. Rios, W. Paulus, A. Cousson, M. Quilichini, G. Heger, N. Le Calve, B. Pasquier, J. Phys. I (Paris) 5 (1995) 763.
[40] K.S. Lee, S.M. Ju, K.L. Kim, S.K. Lee, J.H. Kim, J.B. Kim, B.C. Choi, J.N. Kim, Ferroelectrics 137 (1992) 123.
[41] T. Fernandez-Diaz, A. de Andres, C. Prieto, Ferroelectrics 92 (1989) 71.
[42] B. Pasquier, N. Le Calvé, S. Al Homsi-Teiar, F. Fillaux, Chem. Phys. 171 (1993) 203.
[43] U. Fano, Phys. Rev. 124 (1961) 1866.
[44] J.P. Coignac, H. Poulet, J. Phys. (Paris) 32 (1971) 679.
[45] Z. Ouafik, D. Brulé, F. Romain, B. Pasquier, N. Le Calvé, J. Raman Spectrosc. 27 (1996) 1.
[46] F.K. Vansant, B.J. van der Veken, H.O. Desseyn, J. Mol. Struct. 15 (1973) 425.
[47] A. Matsuo, K. Irokawa, T. Osaka, Y. Makita, J. Phys. Soc. Jpn. 63 (1994) 1626.
[48] A. Novak, Structure and Bonding 18 (1974) 177.
[49] F. Fillaux, B. Marchon, A. Novak, J. Tomkinson, Chem. Phys. 130 (1989) 257.
[50] C. Andreani, P. Bisanti, C. Petrillo, F. Saccheti, B.C. Boland, Z.A. Bowden, A.D. Tayloer, Mol. Phys. 68 (1989) 681.
[51] B. Pasquier, F. Fillaux, J. Tomkinson, Physica B, 213/214 (1995) 658.
[52] F. Fillaux, J. Tomkinson, J. Mol. Struct. 270 (1992) 339.
[53] E. Nakamura, Ferroelectrics 135 (1992) 237.
[54] P. Kubinek, M. Fally, A. Fuith, H. Kabelka, C. Filipic, J. Phys. 7 (1995) 2205.
[55] B. Wyncke, F. Brehat, J. Phys. C: Solid State Phys. 19 (1986) 2649.
[56] M. Fally, A. Fuith, W. Schranz, H. Warhanek, P. Kubinec, C. Filipic, Ferroelectrics 172 (1995) 157.
[57] K. Hayashi, K. Deguchi, E. Nakamura, J. Phys. Soc. Jpn. 57 (1988) 3594.